Journal of
Materials Chemistry A

ROYAL SOCIETY
OF CHEMISTRY

PAPER

View Article Online
View Journal | View Issue

Check for updates

Cite this: *J. Mater. Chem. A*, 2025, **13**, 39001

Zinc alloy dynamic windows with excellent cyclability and thermal stability

Nikhil C. Bhoumik,[a] Samantha M. Thompson,[a] Tyler S. Hernandez[b] and Christopher J. Barile *[a]

Received 9th September 2025
Accepted 27th October 2025

DOI: 10.1039/d5ta07333b

rsc.li/materials-a

Electronically switchable dynamic windows have the promise to significantly reduce energy consumption within buildings and automotive devices. In this paper, we develop Zn electrolytes for reversible metal electrodeposition (RME) windows and improve their thermal bistability and cyclability. By formulating electrolytes that facilitate the reversible electrodeposition of zinc alloys, the dark-state stability of the metal films is significantly improved *versus* the unalloyed systems due to the higher tolerance of the alloys towards water impurities in the DMSO electrolytes. In particular, Zn alloys with Sn and Ni exhibit high dissolution times exceeding 55 h at the ASTM-mandated temperature of 85 °C, 99.2% coulombic efficiency, and 11 000 cycles in 25 cm^2 windows without significant deterioration in optical contrast or switching speed. These innovations bring RME dynamic windows closer to practical adoption and commercialization.

Introduction

Global energy consumption has been steadily increasing, which places a significant strain on resources. The building sector is a major contributor of energy consumption, and buildings currently consume over 40% of energy in the United States.[1] Dynamic windows with electronically switchable transmission are a promising method of decreasing the energy consumption of buildings. These windows, constructed with electronically switchable films, significantly reduce the energy consumption of heating, cooling, and lighting in buildings, leading to an estimated 10–20% energy savings compared to traditional static windows.[2]

While various electrochromic materials have been investigated for dynamic windows, including transition metal oxides,[3] polymers,[4] small molecule organic materials,[5] and plasmonic nanocrystals,[6] these materials face challenges associated with color neutrality, durability, cost-effectiveness, and switching speed. Reversible metal electrodeposition (RME) is an alternative approach for constructing dynamic windows, which offers unique advantages and challenges as compared to electrochromic materials.

RME technology utilizes a transparent conducting electrode, typically tin-doped indium oxide (ITO) coated on glass, that is immersed in an electrolyte containing metal ions. When a voltage is applied, these ions deposit onto the electrode, darkening the window. Reversing the voltage causes the metal to dissolve back into the electrolyte, restoring transparency. The composition of the electrolyte, including the nature of the metal ions, supporting ions, and solvent, is critical in influencing overall device performance. The appearance of the opaque state of the window is controlled by the optical properties of the metals plated onto the working electrode. For most practical window applications, it is desirable for the windows to possess optically transparent electrolytes and color-neutral switching with a clear-to-grey-to-black transition. Additionally, transparent conducting oxides such as ITO are typically unstable under acidic conditions, necessitating the use of pH neutral or alkaline aqueous electrolytes. These optical and stability requirements eliminate the use of Cu, Ag, Bi, and Au in robust aqueous RME electrolytes.[7] On the other hand, Zn-based RME systems are promising due to the colorless nature of Zn^{2+} and the color neutrality of Zn electrodeposits.[8]

Initial investigation into Zn electrolytes focused on water as a solvent, but due to the negative standard reduction potential of Zn ($E^\circ = -0.76$ V *vs.* NHE), H_2 commonly forms as a side product during device switching. Dimethyl sulfoxide (DMSO) has emerged as a promising nonaqueous solvent for RME in dynamic windows, owing to its electrochemical stability, low vapor pressure, and high polarity.[8] Theoretically, DMSO electrolytes containing Zn should not undergo H_2 evolution, thus addressing the primary concern with aqueous systems.

Our research has led to the development of Zn DMSO electrolytes that enable the construction of robust RME windows with impressive optical properties, transitioning from 75% transmission to less than 0.1% opacity. These windows have demonstrated remarkable performance, with first-generation electrolytes (DMSO-1) achieving about 10 000 switching cycles

---

[a] Department of Chemistry, University of Nevada, Reno 89557, Nevada, USA. E-mail: cbarile@unr.edu

[b] Tynt Technologies, Boulder, Colorado, 80301, USA

using complex voltage profiles,[9] and second-generation electrolytes (DMSO-2) reaching approximately 12 000 cycles with constant applied voltages.[8] Additionally, DMSO-1 windows exhibit excellent bistability at room temperature, maintaining their opaque state for up to a month without power input.[9] However, they exhibit poor bistability at elevated temperatures (85 °C).[10] This limitation is significant, as the ASTM-E2141 standard for dynamic windows demands 50 000 cycles without substantial degradation at 85 °C, a benchmark that has not yet been achieved by any RME window.[11] The third generation of electrolytes (DMSO-3), which contains $ZnBr_2$, $Zn(CF_3COO)_2$, and $NaCH_3COO$, cycles about 12 500 times without degradation and demonstrated similar bistability as DMSO-1, with an increased performance at elevated temperatures.

In constructing dynamic windows, achieving bistability and thermal stability is critical. Bistability ensures that the device maintains its opaque or clear state without continuous power input, cycling between states as desired while resisting heat-induced deterioration.[12,13] This characteristic is vital for the uniform behavior of the counter electrode, in which dark-state stability prevents irreversible metal loss, which can lead to metal mesh destruction, device failure, and compromised electrolyte composition over extended cycling.[10] Ideally, the metal mesh used at the counter electrode should narrow upon metal electrodeposition on the working electrode and widen back to its original state when metal is stripped off of the working electrode, allowing for indefinite cycling without deterioration.[10] Although poor bistability does adversely affect device energy consumption, the larger problem is that poor bistability significantly impacts the device's longevity and performance. Therefore, achieving excellent dark-state stability across all operating temperatures is essential for the commercial viability of RME windows.

To address these limitations and push the boundaries of RME technology, we investigate various Zn alloy compositions in DMSO electrolytes in this manuscript. We explore different alloy combinations, chosen for their unique individual properties and potential synergies with Zn. Zn–Ni alloys are highly corrosion-resistant,[14,15] which helps mitigate the destabilizing effects of water impurities in DMSO electrolytes. Water impurities are a key factor in poor bistability, as they can react with Zn to form $Zn(OH)_2$ and other compounds that degrade the electrodeposits. Furthermore, the enhanced deposition efficiency and reliability of Zn–Ni alloys stem from their ability to promote more uniform electrodeposits, reducing the likelihood of dendrite formation and maintaining stable optical performance during cycling. Sn, known for its corrosion-resistant properties, is ideal for enhancing cyclability and longevity, especially when combined with a third alloying element such as Fe or Mn.[14] Zn–Al alloys are similarly corrosion resistant.[15]

Various metal ions, including those of Sn, Mn, Al, Co, Fe, and In were tested individually and in different pairings, and then compared against the previously developed DMSO-1, DMSO-2, and DMSO-3 electrolytes. Sn consistently performed well across trials, but the most significant improvement was observed when paired with Ni. This combination with Zn quintupled the film dissolution time at 85 °C in the newly developed DMSO-3 electrolytes compared to the first and second-generation DMSO electrolytes.

Overall, the DMSO-3-Sn-Ni electrolyte outperforms previous electrolytes, maintaining a continuous metal film at 85 °C for over sixty hours, which is 10 to 20 h longer than DMSO-1 and DMSO-2, and it achieves over 11 700 cycles with a complete switching time between opaque states of 80 s. Furthermore, the DMSO-3-Sn-Ni system maintains a high coulombic efficiency of 99%, which indicates excellent electrochemical reversibility between the Zn electrodeposition and Zn stripping processes. For these reasons, the DMSO-3-Sn-Ni system is a highly promising advancement in the development of robust RME dynamic windows.

Results and discussion

Performance of Zn RME electrolytes

Optimal electrolyte solutions should exhibit certain characteristics to be useful in practical dynamic window applications. In this study, we evaluate the performance of Zn RME electrolytes using three key parameters: coulombic efficiency, dissolution time at 85 °C, and cycle number at 21 °C. These metrics are essential for assessing the practicality and effectiveness of electrolytes in RME dynamic windows.

Coulombic efficiency is defined as the ratio of electric charge extracted during Zn stripping to the charge supplied during Zn electrodeposition. A coulombic efficiency of 100% indicates perfect reversibility, and high coulombic efficiency is crucial for the long-term stability and performance of RME-based dynamic windows.[16] Dissolution time is defined as the total time observed from initial electrodeposition to a film on the working electrode with 0.1% transmission until the films reaches a transmission of 30% while being held in the electrolyte at open circuit potential at 85 °C.[17] Cycle number represents the device longevity at room temperature (21 °C). It is quantified by observing the trend in the maximum and minimum transmission over repeated switching cycles.[8] A RME device is considered to have reached its last cycle number when the contrast ratio, the difference between the maximum and minimum transmission values, falls below 50% of its initial value. An increase in cycle number indicates improved durability and stability of the RME system.

Fig. 1 presents a comparison of these parameters for various electrolyte compositions based on previous research by our group. A previous electrolyte formulated in propionitrile (PrCN) demonstrates promising dissolution time (>25 h) but shows a relatively poor coulombic efficiency of 97% and cycle number of 1050.[10] This suggests that while PrCN may remain stable at high temperatures over time, its overall efficiency and longevity in repeated cycling is limited. The first generation of Zn electrolytes in DMSO (DMSO-1) addresses these issues, exhibiting improved coulombic efficiency (98.5%) and cycle number (7,985), but suffers from low dissolution time (3 h).[9] This tradeoff indicates that while DMSO-1 cycles well, the Zn film exhibits poor dark-state bistability at 85 °C. Subsequent generations of DMSO electrolytes (DMSO-2 and DMSO-3) show steady improvements across all three categories, testifying to the

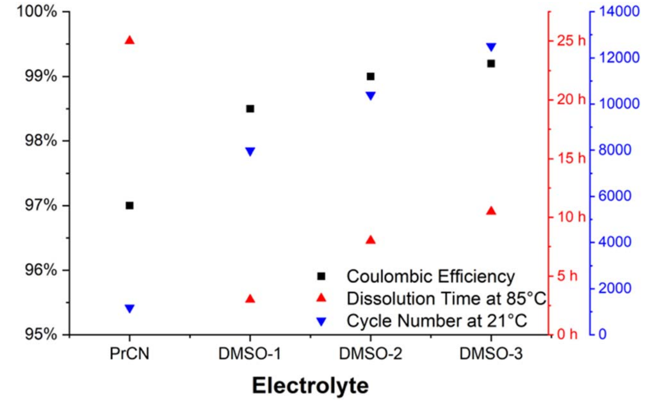

Fig. 1 Comparison of recently developed nonaqueous Zn electrolytes. Coulombic efficiency (black squares), dissolution time at 85 °C (red triangles), and cycle number at 21 °C (blue triangles) of 25 cm^2 dynamic windows using three recently developed nonaqueous Zn electrolytes: PrCN (300 mM $ZnCl_2$, 200 mM LiCl, 25 mM $NaCH_3CH_2COO$, 0.5 wt% PEG), DMSO-1 (300 mM $ZnBr_2$, 300 mM $Zn(CH_3COO)_2$, 400 mM CH_3COONa, 5 wt% polyvinyl alcohol [PVA]), DMSO-2 (300 mM $ZnBr_2$, 200 mM CF_3COOLi, 400 mM HCOOLi, 5 wt% PVA), and DMSO-3 (300 mM $ZnBr_2$, 300 mM $Zn(CF_3COO)_2$, 800 mM CH_3COONa, 5 wt% PVA).

potential of Zn DMSO electrolyte in RME dynamic windows. Of the four compositions examined in Fig. 1, DMSO-3 exhibits the most promising results, achieving the best balance of high coulombic efficiency (99.2%), extended dissolution time (10.5 h), and increased cycle number (12 800). These results demonstrate that careful electrolyte formulation allows for the improvement of all three of these critical parameters.

Building on these comparative results, the DMSO-3 electrolyte contains Zn trifluoroacetate instead of the Zn acetate used in the DMSO-1 electrolyte. We previously demonstrated that Zn acetate is responsible for the formation of $Zn_x(CH_3COO)_{y-z}(OH)_z$ compounds through a partial hydrolysis reaction.[9,18] These Zn hydroxyacetate compounds are insoluble and impede the Zn stripping process, resulting in lower coulombic efficiency in DMSO-1 compared to DMSO-3. Additionally, at elevated temperatures, both Zn and Zn acetate react with water impurities in DMSO, leading to increased formation of $Zn(OH)_2$ and Zn hydroxyacetate compounds and resulting in an increase of insoluble, device-damaging components.[19] This phenomenon explains the observed lower dissolution time for the DMSO-1 electrolyte compared to DMSO-3. The reduced reactivity towards water of the DMSO-3 is due to the lower basicity of the trifluoroacetate (TFA) ion. The presence of three electronegative fluorine atoms in TFA stabilizes its conjugate acid, resulting in a pK_a of approximately 0.5 as compared to 3.75 for formate and 4.76 for acetate.[20–22] This stabilization by the trifluoromethyl group leads to a slower hydrolysis rate.[23–25]

Despite the superior performance in coulombic efficiency, dissolution time, and cycle number, the DMSO electrolytes do not achieve the excellent dark-state bistability at 85 °C that is observed with the PrCN electrolyte.[10] To address this challenge, we study the use of Zn alloys with the DMSO-3 electrolyte to improve its dark-state bistability. The details of this approach and the associated experimental results are elaborated in the following sections.

Improved dark state bistability of Zn alloy systems

Enhancing Zn RME bistability through alloying in DMSO electrolytes. Alloys, which are solid solutions composed of multiple metallic elements, often offer enhanced properties compared to their isolated components, making them an effective strategy for improving dark-state bistability at elevated temperatures in RME devices. More specifically, the benefits of alloying include improved thermal stability, the creation of tailored microstructures, increased corrosion resistance, and synergistic effects that elevate overall material performance.[26] In our study, we investigated the incorporation of small amounts (2.6 mM) of various metal ions into DMSO electrolyte formulations to promote alloy formation during metal electrodeposition. In particular, we explored seven sets of bimetallic (Zn–Co, Zn–Al, Zn–Fe, Zn–Ni, Zn–Mn, Zn–In, Zn–Sn) and trimetallic (Zn–Mn–In, Zn–Ni–Mn, Zn–Sn–In, Zn–Sn–Mn, Zn–Ni–In, Zn–Sn–Al, Zn–Sn–Ni) electrolyte systems.

A key consideration is the potential impact of water impurities on the performance of Zn dynamic windows with DMSO electrolytes. Zn metal is known to react rapidly with boiling water according to eqn (1).[19]

$$Zn + 2H_2O \rightarrow Zn(OH)_2 + H_2 \tag{1}$$

This reaction compromises the bistability of devices at elevated temperatures due to the formation of $Zn(OH)_2$, which can be converted to soluble Zn^{2+} salts *via* ligand-exchange reactions with halides or carboxylates in the electrolyte. Even our DMSO electrolytes that are nominally dried with molecular sieves contain at least 300 ppm water, as reported in our prior work.[10] These water levels are theoretically sufficient to completely dissolve Zn films with 0.1% transmission.[10]

Our results reveal that most metallic additions improve dissolution time across all three generations of DMSO electrolytes, despite the high-water content in some formulations (Fig. S1). This suggests that the improved corrosion resistance of the electrodeposited Zn alloys counteracts the adverse effects of water impurities, thus impeding film dissolution. However, the extended dissolution times observed with the alloy electrolytes were accompanied by a slight reduction in coulombic efficiency compared to the unmodified DMSO-3 and DMSO-1 electrolytes (Fig. 2). The enhanced performance seen with metallic additions, regardless of water content variations, indicates a complex relationship between electrolyte composition and electrochemical behavior.

For example, Zn–Mn alloys, formed by the addition of $MnCl_2$, demonstrated a significant improvement in thermal stability (Fig. S1), increasing dissolution time from 2–3 h to 16 h at 85 °C. This enhancement is likely attributed to the formation of an insoluble passive barrier layer comprised of a manganese oxide, which passivates the surface.[27] Zn–Al alloys, specifically with the addition of $AlCl_3$, demonstrated a moderate improvement in stability, with dissolution times increasing from 2–3 h to approximately 6 h (Fig. S1a). While not as dramatic as some

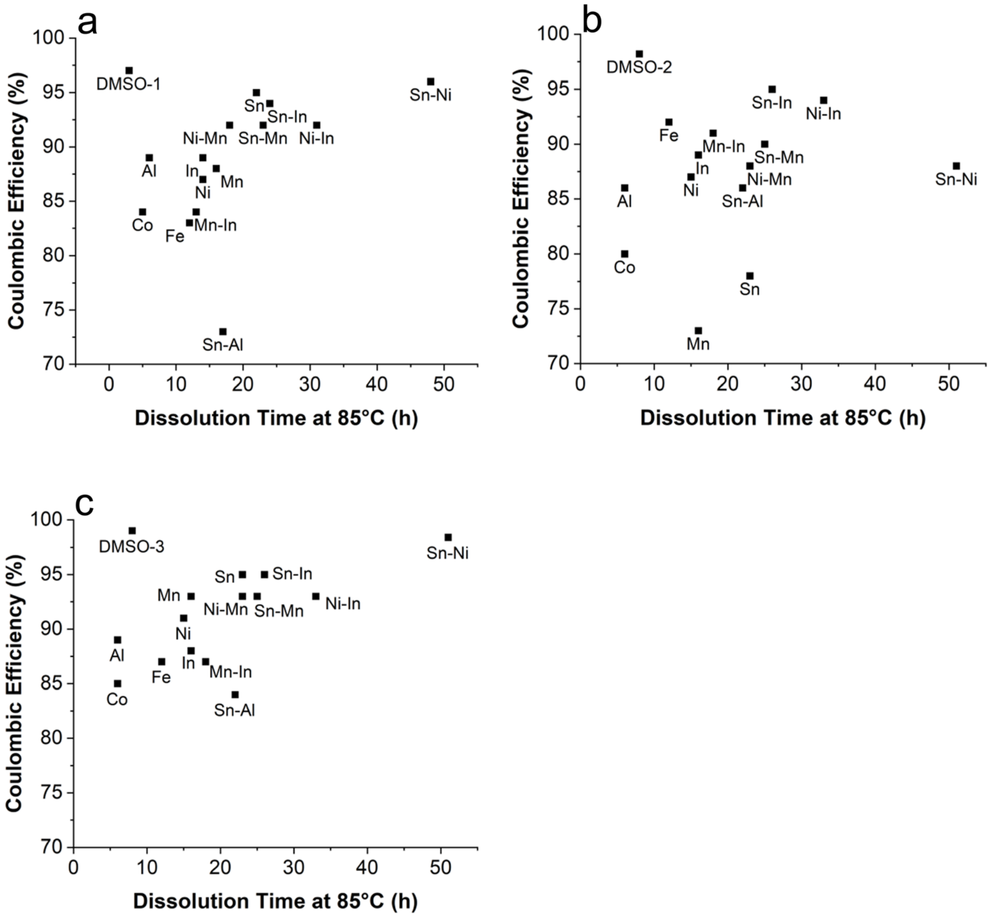

Fig. 2 Coulombic efficiency *vs.* dissolution time. (a) DMSO-1, (b) DMSO-2, and (c) DMSO-3 electrolytes with 2.6 mM other metal halide salt(s). All electrolytes contain 5 wt% PVA. The squares labeled as DMSO-1, DMSO-2, and DMSO-3 without any element refer to the electrolytes without alloys with Zn as the only redox active metal.

other combinations, this improvement aligns with recent battery literature suggesting the potential for dendrite-free behavior in Zn–Al systems.[28] The introduction of $InCl_3$ to form Zn–In alloys resulted in even more significant improvements, with dissolution times extending to approximately 15 h on average in all three generations of DMSO electrolytes (Fig. S1). These findings are consistent with research on various Zn and In alloys, which have shown enhanced stability in different electrolyte systems.[29,30] The substantial increase in dissolution times for Zn–In alloys shows significant improvement in electrochemical stability, likely due to the passivating effect of In imposed by modifying the surface properties of Zn.[28,31] Interestingly, Sn–Ni alloy systems showed distinct behavior when compared across DMSO-1 and DMSO-3 electrolytes. Specifically, the Sn–Ni combination exhibits dissolution times approaching 48 h in DMSO-3 while maintaining comparable coulombic efficiency values as both the unmodified DMSO-1 and DMSO-3 electrolytes (Fig. 2).

Tian *et al.* demonstrated that a three-dimensional Zn–Cu alloy effectively regulates Zn plating and stripping processes in aqueous Zn-ion batteries, suppressing dendrite growth and improving overall battery performance.[31] Similarly, Wang *et al.* reported that surface patterning of Zn electrodes with a localized Zn–In interface significantly improves the cycling stability and rate capability of aqueous Zn-ion batteries.[32] Zn–Ni alloys have garnered considerable attention due to their enhanced corrosion resistance, ductility, and ability to reduce hydrogen embrittlement.[33] Although Zn electrodeposition tends to dominate over Ni in co-deposition processes, suggesting that Ni would be inconsequential in the presence of Zn, the addition of 2.6 mM $NiCl_2$ increased dissolution times to approximately 14 h in DMSO-1 and about 8 h in the other two DMSO electrolytes, demonstrating the effectiveness of Ni as an alloying element (Fig. 2 and S1).

Interestingly, several of the ternary alloys outperformed binary alloys. For example, the $SnCl_2$–$NiCl_2$ combination exhibits the best overall performance, with dissolution times of 48 h in DMSO-1, 51 h in DMSO-2, and 55 h in DMSO-3 electrolytes (Fig. 2 and S1). Other noteworthy combinations, such as $SnCl_2$–$InCl_3$ and $SnCl_2$–$MnCl_2$, also show significant improvements in stability compared to their respective binary alloys. These studies collectively highlight how alloying can significantly impact electrochemical performance in RME electrolytes.

Electrochemical characterization and optical performance of DMSO-3-Sn-Ni electrolyte. Building on previous research with Zn DMSO electrolytes,[8,9,34] we developed DMSO-3, a new formulation containing $ZnBr_2$, $Zn(CF_3COO)_2$, and $NaCH_3COO$. This composition was inspired by earlier studies on aqueous Zn electrolytes, which demonstrated that mixtures of Zn halides, Zn carboxylates, and Na carboxylates can yield highly reversible Zn electrodeposition.[35]

Cyclic voltammetry (CV) coupled with *in situ* transmission measurements serves as a powerful tool for characterizing RME electrolytes for dynamic window applications.[36] This approach enables simultaneous study of electrochemical reactions and optical properties during cycling, facilitating the development of high-performance electrolyte formulations. We employed this technique to characterize the DMSO-3 electrolyte and its variants. Fig. 3a presents CVs of Zn electrodeposition and stripping on Pt-modified ITO electrodes using various electrolyte compositions. The ITO is modified with Pt nanoparticles to enhance nucleation kinetics and electrodeposit uniformity as has been discussed in previous RME systems.[8] During the initial negative-going voltage sweep, cathodic current initiates Zn electrodeposition. The DMSO-3 electrolyte (red line, Fig. 3a) exhibits a more positive onset potential (−0.16 V) compared to a simple $ZnBr_2$ electrolyte (−0.39 V *vs.* Zn/Zn^{2+}, black line), indicating substantially improved electrodeposition kinetics. This enhancement can be attributed to the synergistic effects of the multiple ionic species present in the DMSO-3 formulation.

To further optimize the electrolyte, we investigated the impact of adding small amounts (2.6 mM each) of Sn and Ni salts to DMSO-3. The addition of $SnCl_2$ (blue line), $NiCl_2$ (green line), and their combination (purple line) resulted in onset potentials of −0.13 V, −0.21 V, and −0.10 V, respectively (Fig. 3a). These variations in onset potentials suggest that the additives play distinct roles in modifying the electrodeposition process. Individually, the Sn^{2+} additive appears to facilitate Zn nucleation, while Ni^{2+} shows a less pronounced effect. However, the synergistic combination of both Sn^{2+} and Ni^{2+} results in the most positive onset potential, indicating a complex interaction between these species during the initial stages of Zn electrodeposition. These additives likely influence the nucleation and growth processes of Zn, potentially through mechanisms such as co-deposition, underpotential deposition, or modification of the electrode surface energy.

Fig. 3b displays the corresponding optical transmission data at 600 nm for each electrolyte composition. The transmission decreases as metal deposition occurs and returns to near-original values after stripping, demonstrating the reversible nature of the electrodeposition process. Notably, the DMSO-3 electrolytes with Sn and Ni additives show distinct optical responses. For these electrolytes, the transmission of the electrode decreases to below 0.1% during metal deposition and then returns to near its original value after stripping (Fig. 3b, purple line). This observation suggests that these elements influence not only the electrochemical process but also the morphology and optical properties of the deposited films.

In contrast, while the electrode using only the DMSO-3 electrolyte achieves a comparable level of darkening, it fails to recover its original transmission value after metal stripping (Fig. 3b, red line). The DMSO-Sn-Ni electrolyte exhibits a darkening that is approximately 12 s faster than the unmodified DMSO-3 electrolyte and demonstrates slightly enhanced optical reversibility. The accelerated darkening rate in the presence of $SnCl_2$ and $NiCl_2$ suggests that these additives enhance the compactness of Zn electrodeposits on the ITO substrate, resulting in a denser and faster darkening process. Comparing Zn electrodeposits formed from the combination of $SnCl_2$ and $NiCl_2$ in DMSO-3 to those formed from individual components reveals more efficient light blocking with the Zn–Sn–Ni electrodeposits as evidenced by scanning electron microscopy (SEM) imaging (Fig. 4 and S2). The DMSO-3 electrolyte containing both 2.6 mM $SnCl_2$ and 2.6 mM $NiCl_2$ (Fig. 3a, purple line) demonstrates excellent electrochemical reversibility, with a coulombic efficiency of approximately 99%. This high efficiency indicates nearly complete utilization of the deposited Zn

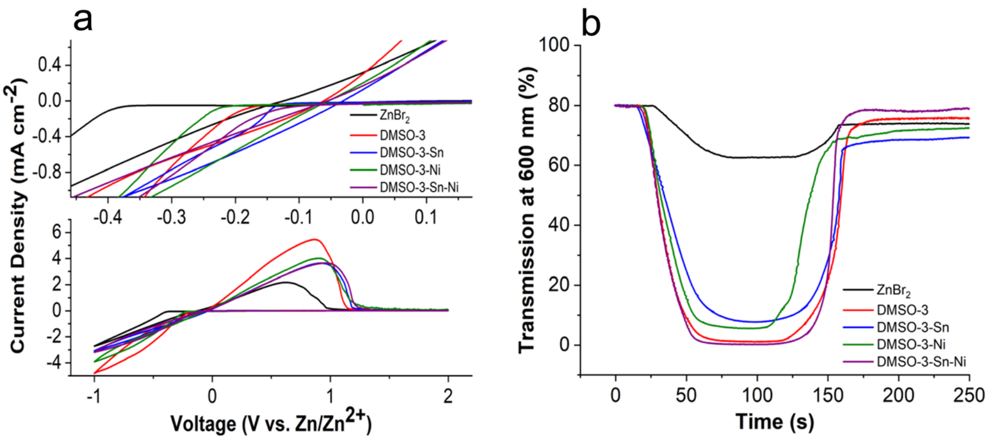

Fig. 3 Cyclic voltammograms and transmission of Pt-modified ITO in DMSO-3-Sn-Ni electrolytes. Cyclic voltammograms (a) and corresponding transmission at 600 nm (b) of Pt-modified ITO electrodes at a scan rate of 20 mV s^{-1} in a 300 mM $ZnBr_2$ electrolyte (black line), the DMSO-3 electrolyte containing 300 mM $ZnBr_2$, 300 mM $Zn(CF_3COO)_2$, and 800 mM $NaCH_3COO$ (red line), a DMSO-3 electrolyte with 2.6 mM $SnCl_2$ (blue line), a DMSO-3 electrolyte with 2.6 mM $NiCl_2$ (green line), and a DMSO-3 electrolyte containing both 2.6 mM $SnCl_2$ and 2.6 mM $NiCl_2$ (purple line).

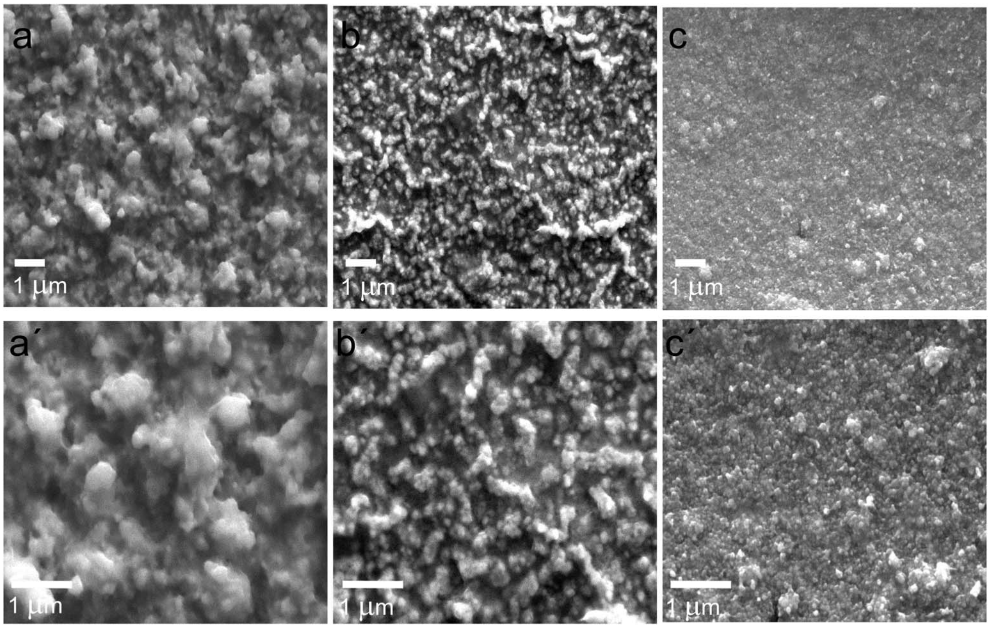

Fig. 4 Scanning electron micrographs of Zn electrodeposits produced from DMSO-3 electrolytes using chronoamperometry at −0.9 V until electrode transmission is equal to 1%. Electrodeposits produced from a DMSO-3 electrolyte containing 300 mM $ZnBr_2$, 300 mM $Zn(CF_3COO)_2$, 800 mM $NaCH_3COO$ with 2.6 mM $SnCl_2$ (a and a′), a DMSO-3 electrolyte containing 300 mM $ZnBr_2$, 300 mM $Zn(CF_3COO)_2$, 800 mM $NaCH_3COO$ with 2.6 mM $NiCl_2$ (b and b′), and a DMSO-3 electrolyte containing 300 mM $ZnBr_2$, 300 mM $Zn(CF_3COO)_2$, 800 mM $NaCH_3COO$ with 2.6 mM $SnCl_2$ and 2.6 mM $NiCl_2$ (c and c′).

during the stripping process, which is crucial for the long-term stability and performance of dynamic window devices.

Zn electrodeposit morphology and alloy formation. SEM images (Fig. 4) illustrate the significant influence of $SnCl_2$ and $NiCl_2$ additives on the surface morphology of Zn electrodeposits formed in the Zn-DMSO electrolyte. The morphological variations indicate that these additives play a crucial role in determining the structure of the Zn deposits. When the dynamic window is tinted to 10% transmission, the Zn deposits exhibit a relatively smooth surface with minimal nanoscale openings (Fig. S2). This smooth morphology is vital for efficient light blocking, which contributes to the high opacity observed in the devices.[9] At lower transmission levels (1% transmission), the Zn electrodeposits experience further morphological changes, in which a secondary layer of rougher surfaces forms over the smooth underlayer (Fig. 4).

In Fig. 4(a and a′), the Zn deposits produced with $SnCl_2$ show a rough, granular structure with uneven Zn clusters, indicative of non-uniform electrodeposition. Similarly, the deposits produced with $NiCl_2$, shown in Fig. 4(b and b′), display a morphology with smaller, irregular electrodeposits. In contrast, the combined use of $SnCl_2$ and $NiCl_2$ in the DMSO-3 electrolyte, shown in Fig. 4(c and c′), results in significantly smoother and more uniform Zn deposits. The synergistic interaction between Sn and Ni appears to promote more controlled nucleation and growth processes, leading to a more cohesive and minimally rough surface. This improved surface morphology is critical for dynamic window applications, where smooth surfaces enhance opacity. The enhanced smoothness and uniformity of the Zn deposits resulting from the combined use of $SnCl_2$ and $NiCl_2$ also improve chemical and electrochemical stability. These smoother surfaces are less prone to defects, cracks, or other structural weaknesses that could lead to corrosion or mechanical failure during cycling. The superior performance of these deposits, demonstrated by longer dissolution times and higher coulombic efficiencies, as described in the Improved dark state bistability of Zn alloy systems section, underscores the advantages of using a Sn–Ni combination for Zn electrodeposition.

We hypothesize that the exceptional bistability and durability of the Zn–Sn–Ni system originate from synergistic alloy-phase formation and interfacial stabilization that have been witnessed in other eletrodeposition contexts. During electrodeposition, Sn^{2+} undergoes underpotential reduction on Zn surfaces to form Zn–Sn intermetallic nuclei (Zn_2Sn) that act as chemically inert seeds and suppress water-driven hydrolysis and $Zn(OH)_2$ formation.[29,37] Ni^{2+} concurrently promotes homogeneous nucleation and incorporates into solid-solution phases with Zn (γ-Ni_2Zn_{11}, Ni_5Zn_{21}), refining the grain structure and mitigating localized current–density fluctuations.[16,33] These dual effects yield compact, adherent films that restrict solvent access and resist thermal degradation, consistent with the markedly longer dissolution times observed at 85 °C. Isolated Sn typically crystallizes in a tetragonal β-Sn structure and forms hundreds-of-nanometer-sized agglomerates that create discontinuous surfaces and limit uniform deposition.[38] However, when Ni is introduced, the resulting Sn–Ni alloy adopts smaller, tens-of-nanometer cubic clusters that unify the surface and provide three-dimensional symmetry, leading to reproducible switching and enhanced device longevity. This improvement is consistent with the stronger Sn–Ni interaction, as evidenced by SEM imaging (Fig. 4) and by prior reports of a negative deviation from Vegard's law for Sn–Ni alloys, indicating lattice contraction and stronger atomic bonding.[39,40] Together, these structural and electronic effects give rise to smoother electrodeposits, higher interfacial stability, and improved thermal bistability. Similar alloy-assisted stabilization has been reported for Zn–Sn–Ni corrosion-resistant coatings,[14] findings that support Sn–Ni co-alloying fundamentally enhancing both thermal bistability and long-term reversibility in RME windows.

Additionally, energy-dispersive X-ray (EDX) and X-ray diffraction (XRD) analyses were conducted to further classify and understand the composition and crystal facets of the Zn–Sn–Ni electrodeposits. Due to the presence of Sn in the electrolyte, as well as in the ITO-coated glass used within the window devices, experiments were conducted on both ITO-coated glass and Cu substrates devoid of Sn. EDX data confirm the presence of Zn, Sn, and Ni in the electrodeposits (Fig. S3a). While XRD results show distinctive peaks corresponding to Zn, Sn, and Ni, the spectra are complex. The XRD spectrum of DMSO-3 electrolyte with Sn–Ni (Fig. S3e) on Cu has additional peaks at unique intensities not present in spectrum of unmodified DMSO-3 on Cu (Fig. S3b), the DMSO-3 with Sn on Cu XRD spectrum (Fig. S3c), and the DMSO-3 with Ni on Cu XRD spectrum (Fig. S3d). Because the XRD spectrum of the DMSO-3 electrolyte with Sn and Ni is distinct from DMSO-3 with only Sn and only Ni, the distinct peaks in the Zn–Ni–Sn spectrum could potentially be assigned to intermetallic phases although there is some ambiguity to these assignments due to complexity of the spectra. A complete list of the possible peak assignments for the XRD spectra is given in Table S1.

Practical two-electrode Zn–Sn–Ni dynamic windows

Impact of electrolyte viscosity on Zn–Sn–Ni electrolytes. The incorporation of polymers into RME electrolyte offers multiple benefits. Viscous electrolytes, such as those containing hydroxyethylcellulose (HEC) and polyvinyl alcohol (PVA), not only enhance safety by reducing leakage risk in the event of window breakage, but also facilitate the manufacturing process.[41] For these reasons, it is important to consider the effects of electrolyte viscosity on electrodeposition and optical performance. Fig. 5 highlights the influence of different PVA concentrations in the DMSO-3-Sn-Ni electrolyte.

Higher viscosity generally results in reduced ionic conductivity, which can slow metal electrodeposition.[42] Despite this tradeoff, PVA and HEC are known to improve the morphology of Zn electrodeposits, leading to enhanced light-blocking efficiency during the dynamic switching process.[7,41] This positive impact on morphology can, in many cases, outweigh the drawbacks of slower deposition kinetics, ultimately enhancing the overall switching speed of the electrolyte.[41]

The cyclic voltammograms in Fig. 5a demonstrate that increasing PVA concentration from 2 wt% to 10 wt% reduces the magnitude of the current density, which is consistent with the expected decrease in ionic conductivity with increased viscosity. However, the electrolyte containing 5 wt% PVA shows superior optical reversibility and coulombic efficiency (99.2%), indicating that this concentration strikes an optimal balance between enhancing Zn electrodeposit morphology and maintaining effective electrochemical performance.

Furthermore, the optical switching behavior, depicted in Fig. 5b, shows that 5 wt% PVA enables faster darkening and stripping kinetics relative to other electrolytes. In contrast, 10 wt% PVA negatively impacts optical reversibility, likely due to excessive viscosity, which overly hinders ion transport. This pattern aligns with previous research, which found that high polymer concentrations slow deposition kinetics and degrade the quality of Zn electrodeposits.[7,8,38] Due to the optimal spectroelectrochemical performance of the electrolyte with 5 wt% PVA, we went on to study the optical performance of two-electrode Zn–Sn–Ni dynamic windows.

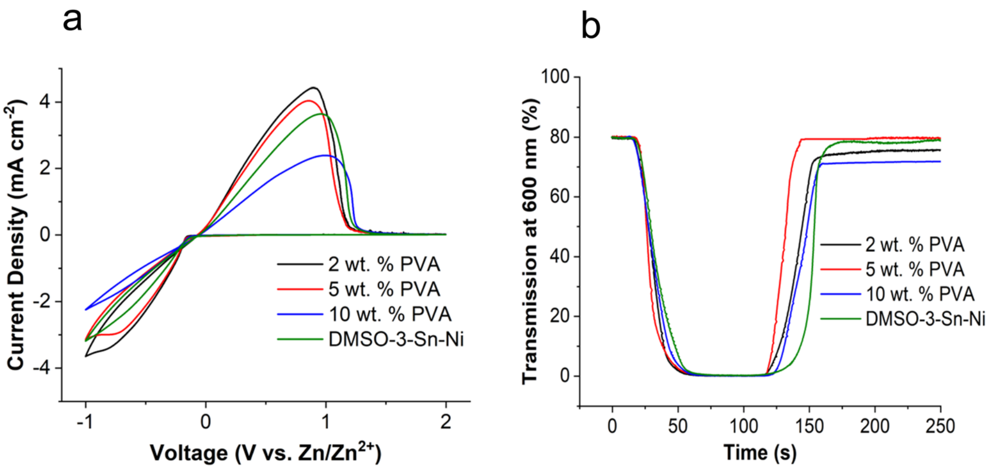

Fig. 5 Effect of PVA concentration on the electrochemical and optical performance of Zn-alloy dynamic windows in DMSO-3-Sn-Ni electrolyte. (a) Cyclic voltammograms of Zn electrodeposition and stripping on Pt-modified ITO electrodes in DMSO-3-Sn-Ni electrolyte with 2 wt% PVA (black line), 5 wt% PVA (red line), 10 wt% PVA (blue line) and DMSO-3-Sn-Ni electrolyte without PVA (green line) at a scan rate of 20 mV s^{-1}. (b) Corresponding transmission measurements at 600 nm.

Optical properties of two-electrode Zn–Sn–Ni dynamic windows. The data in Fig. 6a illustrate that there is a significant decrease in transmission across the visible spectrum (400–800 nm) as the tinting time of the 100 cm^2 device increases. The transmission starts at approximately 63% at 0 s and declines to below 5% after 40 s, reaching nearly 0% after 300 s, due to the formation of a highly opaque Zn metal layer. The outdoor reflection (Fig. 6b), in which light is illuminated at the ITO working electrode side of the device exhibits higher reflection across all wavelengths compared to the indoor side (Fig. 6c), in which light is illuminated at the glass and metal mesh counter electrode side of the device. The smoother base of the metal electrodeposits and the fact that the light has a shorter path length because it does not have to pass through the electrolyte results in a greater amount of reflection in the outdoor orientation. This orientation-dependent reflection is consistent with previous studies on RME devices.[43] Initially, at 0 s, the outdoor reflectance is around 15%, and as tinting time progresses, it rises dramatically to between 60–80% after 300 s. By combining smoother Zn electrodeposition from the PVA-enhanced electrolyte and optimizing the reflection properties based on the direction of incident light, the dynamic windows achieve enhanced energy savings potential due to their ability to reject light and heat from visible and near-infrared light.

To assess the heat modulation capabilities of the windows in a practical building environment, we determined the solar heat gain coefficients (SHGCs) of the Zn–Sn–Ni windows in a modeled insulated glass unit (Fig. S4). The SHGC of the practical window unit in its opaque state (300 s of electrodeposition) is only 0.049, which indications that the majority of the solar heat gain would be blocked by the electrodeposited Zn–Sn–Ni film (Table S2). With the same IGU stack, the modeled SHGC with a Generation 4 dynamic film from View, Inc. in its darkest state is 0.091. These findings indicate that the Zn–Sn–Ni RME chemistry developed in this work is predicted to outperform the heat-modulation abilities of state-of-the-art commercial dynamic windows.

In addition to reflection, the energy efficiency of dynamic windows also depends on their power consumption. The DMSO-3-Sn-Ni dynamic windows, covering an area of 100 cm^2, require only an average power of just 6 W m^{-2} during the tinting process to achieve less than 5% transmission in the visible range. This power requirement is comparable to that of a single household LED light bulb for a 1 m^2 window.[44] Notably, these dynamic windows exhibit remarkable bistability at both room temperature and 85 °C, meaning no energy is needed to maintain either the clear or dark state. For instance, after 300 s of tinting, the transmission remains low at less than 0.5%, even

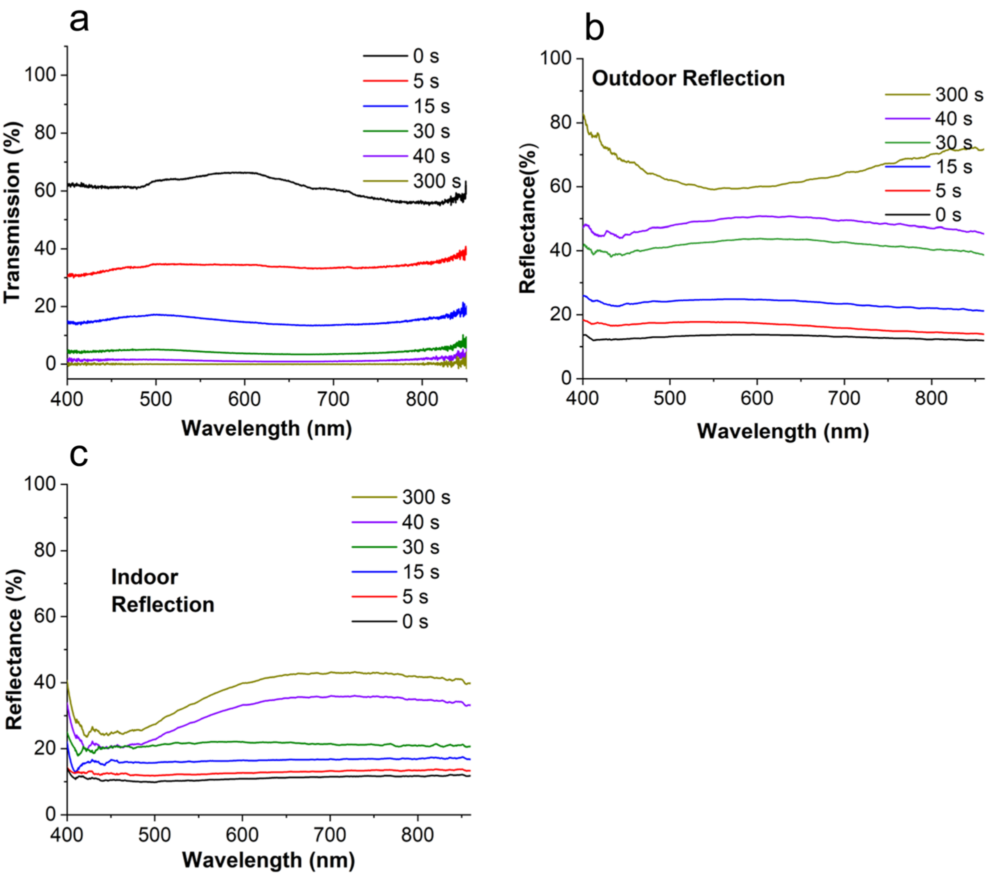

Fig. 6 Device optical properties. Transmission (a), outdoor reflectance (b), indoor reflectance (c) of a two-electrode 100 cm^2 Zn dynamic window using a DMSO-3-Sn-Ni electrolyte containing 300 containing 30 mM $ZnBr_2$, 30 mM $Zn(CF_3COO)_2$, 80 mM $NaCH_3COO$, 2.6 mM $SnCl_2$ and 2.6 mM $NiCl_2$ with 5 wt% PVA after tinting at −0.8 V for 0 s (black), 5 s (red), 15 s (blue), 30 s (green), 40 s (purple) and 300 s (dark yellow).

after being left unplugged for 55 h at 85 °C (Fig. S5). This improvement in bistability was also observed with previously developed electrolytes (DMSO-1 and DMSO-2) containing small amounts of $SnCl_2$ and $NiCl_2$ (Fig. S5), but their cycling performance is not equivalent, as discussed in the next section.

Cyclability of Zn–Sn–Ni dynamic windows. Having established the enhanced bistability and thermal stability of the DMSO-3-Sn-Ni electrolyte, we now turn our focus to the cycling durability of windows containing the Zn–Sn–Ni electrolytes. Long-term cyclability remains a critical challenge for dynamic windows, especially when both extended cycling and thermal stability are needed. In previous studies, Zn-based dynamic windows using DMSO electrolytes demonstrated cycling up to 10 000 cycles with reasonable stability.[8,9] However, by incorporating Sn and Ni to form a Zn–Sn–Ni alloy, we have surpassed this performance. In this work, dynamic windows with DMSO-3-Sn-Ni electrolyte were cycled at −0.8 V for 30 s and +1.0 V for 60 s, maintaining stable dark state transmission over 11 700 cycles (Fig. 7c). This represents a significant advancement in RME windows, progressing toward the ASTM standard of 50 000 cycles for commercial viability.[11]

In comparison, Fig. 7a presents the cycling performance of DMSO-1-Sn-Ni over 5451 cycles, in which a modest increase in minimum transmission attained during each cycle is observed. Fig. 7b highlights DMSO-2-Sn-Ni, which achieves 8200 cycles, but some degradation occurs after ∼6000 cycles. In contrast, DMSO-3-Sn-Ni outperforms both, demonstrating consistent cycling behavior without significant degradation.

The superior performance of DMSO-3-Sn-Ni is largely attributed to the enhanced morphology of the Zn electrodeposits, achieved through the addition of 5 wt% PVA, $SnCl_2$, and $NiCl_2$. As discussed previously, the Zn–Sn–Ni electrolyte improves the bistability and thermal stability of the dark state film, particularly at high temperatures (up to 85 °C). When compared to the cycling capabilities of DMSO-only systems, such as those shown in Fig. S6 (without $SnCl_2$ and $NiCl_2$), the advantages of the Zn–Sn–Ni electrolyte become even more apparent. While DMSO-3 without $SnCl_2$ or $NiCl_2$ performs well up to 12 000 cycles, its optical reversibility, thermal stability and dark state bistability at 85 °C are less consistent than the DMSO-3-Sn-Ni system. Thus, the DMSO-3-Sn-Ni system demonstrates a balanced electrolyte composition, offering improved Zn electrodeposition and extended cycling durability, making it a more suitable option for dynamic window applications requiring long-term optical and thermal stability.

Switching uniformity of 100 cm^2 Zn–Sn–Ni dynamic windows. Uniform switching across large-area windows is a critical challenge for the commercialization of dynamic windows. In RME windows, achieving aesthetically pleasing variable transmission control requires uniform metal electrodeposition across the electrode surface. Notably, the rate of metal electrodeposition on the electrode must be constant

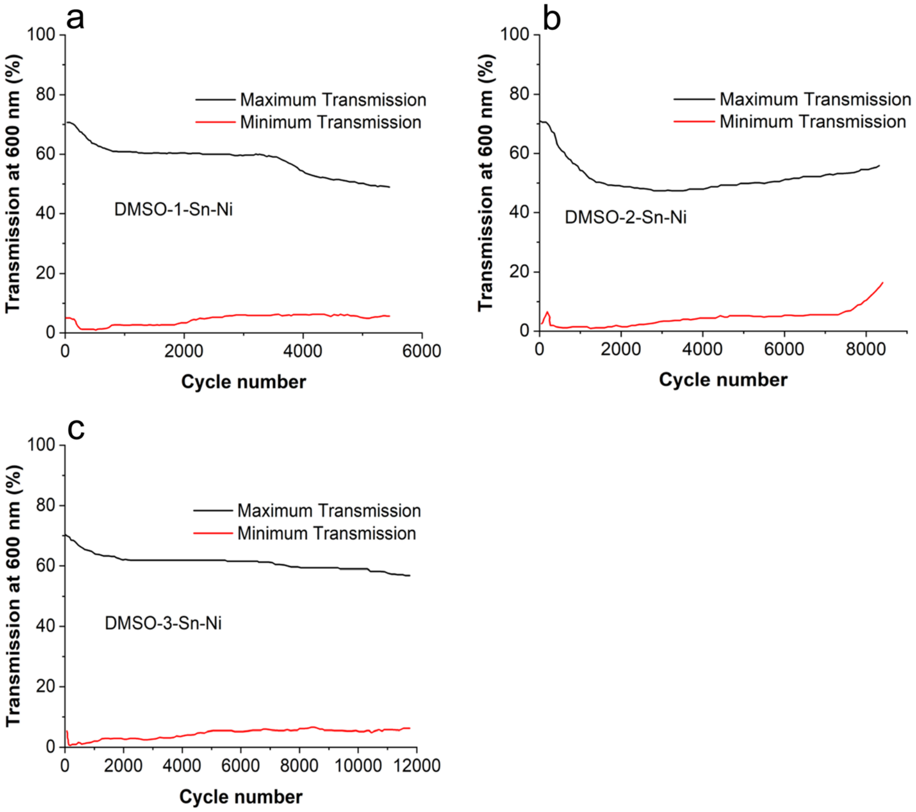

Fig. 7 Minimum and maximum transmission at 600 nm of 25 cm^2 dynamic windows during cycling using various Zn DMSO electrolytes. The windows contain $NiCl_2$, $SnCl_2$, and 5 wt% PVA with the DMSO-1 (a), DMSO-2 (b), and DMSO-3 (c) formulations. In all cases, each switch cycle consisted of −0.8 V for 30 s to induce device darkening followed by +1.0 V for 60 s to induce device lightening.

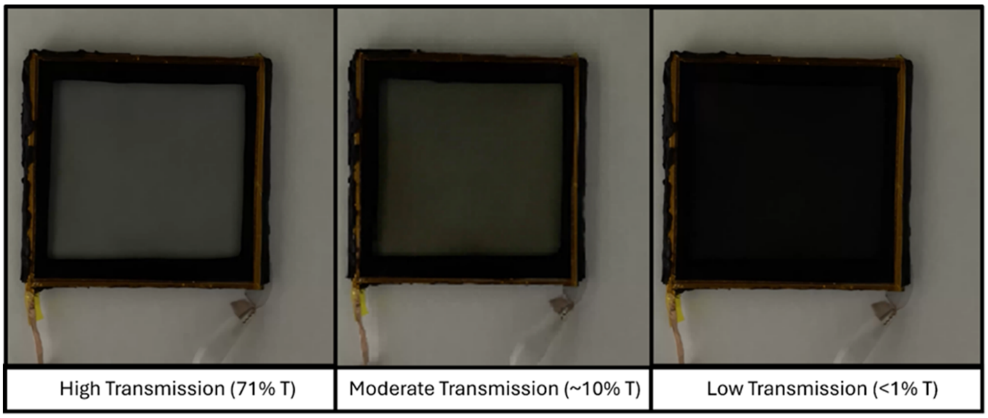

Fig. 8 Photographs of a 100 cm^2 dynamic window device at different optical transmission states using tinting at −1.2 V for 30 s and clearing at +1.2 V for 60 s. From left to right: clear state (71% transmission at 600 nm), moderate tint state (∼10% transmission at 600 nm after 15 s of electrodeposition), and dark state (∼1% transmission at 600 nm after 30 s of electrodeposition).

across all points independent of voltage drops induced by fluctuating localized currents during cycling. A characteristic of the electrolyte that promotes ideal metal electrodeposition behavior is having sufficient diffusion to limit metal ion deposition rate on the electrode. This diffusion-limited electrodeposition allows for the rate of tinting to be unaffected by voltage drop across the electrode caused by the non-negligible sheet resistance of transparent conductors such as ITO on glass, which can enable uniform device switching.

The data in Fig. S7 demonstrate that the tinting speed increases as the voltage becomes more negative, transitioning from −0.6 V to −1.0 V. However, from −1.0 V to −1.4 V, the tinting speed remains relatively unchanged (Fig. S7b). This observation suggests that, within this voltage range, Zn electrodeposition is limited by the diffusion of Zn^{2+} ions to the electrode, rendering it insensitive to variations in electrode polarization. This interpretation is supported by a diffusion-limited peak observed in the CV of the diluted (60 mM and 30 mM Zn^{2+}) DMSO-3-Sn-Ni electrolytes around −1.0 V *vs.* Zn/Zn^{2+} (Fig. S8).

This diffusion-limited characteristic of the dilute electrolyte proves advantageous for uniform tinting over large areas. For a window area of 100 cm^2, our calculations of voltage distribution, considering the transparent electrode's sheet resistance (10 Ω sq^{-1}) and the average current density (1.01 mA cm^{-2}) required for switching at −1.2 V, indicate that that the maximum voltage drop across the ITO electrode is 0.13 V (Fig. S9). This voltage drop implies that uniform switching should occur across the 100 cm^2 electrode due to the diffusion-limited nature of the dilute DMSO-3-Sn-Ni electrolyte because the effective voltage going towards metal electrodeposition from the edge (−1.2 V) to the center of the device (−1.07 V) lies within the diffusion-limited range of voltages.[45]

To validate these predictions, we constructed 100 cm^2 Zn DMSO windows using a transparent Zn metal mesh as the counter electrode. Optical measurements, photographs, and videos demonstrate excellent switching uniformity at this scale (Fig. 6 and 8, Video S1).

To benchmark the performance of the Zn–Sn–Ni alloy electrolyte against other state-of-the-art electrochromic and RME dynamic windows, a comprehensive comparison of reported systems is provided in Table S3. The Zn–Sn–Ni system developed in this work exhibits a coulombic efficiency of 99.2%, promising cycling durability of ∼11 700 cycles, and remarkable thermal bistability of 55 h at 85 °C, surpassing previously reported Zn-based electrolytes and other RME devices. The optical contrast (∼70%) and rapid switching time (∼5 s) also place this system among the fastest RME windows reported. Collectively, these metrics highlight the synergistic advantages of Sn and Ni co-alloying in achieving high stability, strong optical modulation, and superior thermal tolerance relative to existing dynamic window technologies although more advancements will be needed for these windows to rival the cycling durability of commercial WO_3 electrochromics.

Conclusions

In summary, we report a Zn–Sn–Ni alloy electrolyte that enables highly reversible, thermally stable, and color-neutral dynamic windows based on RME. Co-alloying Zn with Sn and Ni markedly enhances interfacial stability and suppresses dendritic growth, achieving a coulombic efficiency of 99.2%, long-term durability over ∼11 700 cycles, and exceptional bistability of 55 h at 85 °C. These results represent a significant advancement over previous Zn-based electrolytes and RME systems, establishing alloy chemistry as a versatile route for designing durable and fast-switching dynamic windows. Future studies will focus on tuning alloy compositions and polymeric host environments to further improve switching kinetics, optical neutrality, and large-area device integration for sustainable building applications.

Experimental procedures

General procedures

Chemicals were procured from commercial suppliers without further purification unless specified otherwise. Anhydrous

DMSO was obtained from DMSO Store, Inc. and anhydrous CH_3CN from Sigma Aldrich were dried over 4 Å molecular sieves from Oakwood Chemical for a minimum of one week. The anhydrous salts used in the DMSO electrolytes were stored in an Ar-filled glove box, maintaining conditions of less than 1 ppm O_2 and less than 0.1 ppm H_2O.

Metal chlorides were sourced as follows: $AlCl_3$ and $SnCl_2$ (97%, ACROS Organics), $MnCl_2$ and $InCl_3$ (Oakwood Chemical), $CoCl_2$ (Baker Chemical), and $FeCl_3$ (Loudwolf Industrial Scientific). Sodium acetate (98%) was obtained from Thermo Fisher Scientific Chemicals. Additionally, PVA with a molecular weight range of 31 000–50 000 was purchased from Sigma Aldrich. Moreover, $ZnBr_2$ and $ZnCF_3COO$ (99%) were procured from Oakwood Chemical. Tin-doped indium oxide on glass substrates (10 Ω sq^{-1}) were sourced from Xin Yan, Inc. Additionally, an aqueous dispersion of Pt nanoparticles (3 nm in diameter, 1000 ppm) was procured from US Research Nanomaterials, Inc.

Electrochemical methods

All electrochemical measurements were conducted using a VSP-300 Biologic potentiostat. A three-electrode configuration was utilized for cyclic voltammograms, featuring a transparent conducting working electrode alongside high-purity Zn foil (99.99% from Leishent) as both counter and reference electrodes. The transparent conducting working electrodes were composed of ITO on glass modified with Pt nanoparticles (3 nm in diameter, Sigma Aldrich). These Pt nanoparticles acted as inert seed layers to promote uniform nucleation during the redox-mediated electrochemical (RME) process, following established methodologies in the literature.[45] To evaluate the optical properties of the electrochemical systems, transmission measurements were conducted concurrently with cyclic voltammetry using a 2 cm by 2 cm glass cuvette with an immersed working electrode area of 2.4 cm^2.

Thermal stability tests

Zn alloy electrodeposits were produced on 2 cm by 2 cm Pt-coated ITO glass substrates using chronoamperometry at −0.9 V for 300 s. Immediately after deposition, the plated ITO glass was transferred to a 10 mL sealed vial containing the corresponding electrolyte maintained at 85 °C. The film dissolution time was recorded when approximately 30% of the film had dissolved.

Water content analysis

The water content of the electrolytes was quantified using ^1H NMR spectroscopy. Electrolyte samples were diluted thirteen-fold with DMSO-d_6, and 10 µL of acetonitrile (CH_3CN) was added as an internal standard before analysis.

Device construction

Dynamic two-electrode windows were constructed using a working electrode of Pt-modified ITO on glass, paired with a Zn grid counter electrode on a glass backing. For the 25 cm^2 windows, a commercially available Zn grid (Kwikmesh) with approximately 1 cm interwire spacing and a 3 mm wire diameter was utilized. To enhance the aesthetic appeal of the transparent Zn grids, we fabricated grids starting from commercially available Cu mesh (TWP, Inc.). The fabrication process involved several steps and was described in depth previously.[9] All windows were sealed around the electrode perimeter using butyl rubber (Solargain, Quanex, Inc.). The final step involved injecting the electrolyte into the devices through the butyl rubber sealant using a syringe and a 22-gauge needle, achieving an electrolyte thickness of approximately 1.5 mm.

Materials characterization

Visible light transmission measurements were performed using an Ocean Optics FLAME-S-VIS-NIR spectrometer in conjunction with an Ocean Insight HL2000-FHSA light source. Reflection measurements were conducted with an Ocean Insight reflection probe. For two-electrode device measurements, 100% transmission was defined as the transmission of open air. For the 25 cm^2 windows, transmission data were recorded at the center of the device through an open area in the Zn grid, though some light was obstructed by the grid lines, resulting in slightly lower maximum transmissions compared to the clear-state values in the three-electrode measurements. In contrast, the 100 cm^2 windows, which utilized transparent Zn meshes with smaller grid lines, provided transmission values that accounted for any mesh opacity. SEM and EDX analyses were conducted using a JEOL JSN-7100F field emission SEM at an acceleration voltage of 15 kV. ^1H NMR spectra were recorded using a Varian 400 MHz NMR Spectrometer, with chemical shifts referenced to the protio solvent peak at 2.50 ppm in DMSO-d_6. Photographs of the dynamic windows were taken with a Google Pixel 5a smartphone.

Conflicts of interest

N. C. B. and C. J. B. have submitted a patent application covering aspects of the work described in this manuscript. T. S. H. is a cofounder of Tynt Technologies, Inc., a company commercializing dynamic windows. C. J. B. serves as an advisor to Tynt Technologies, Inc. No additional conflicts of interest are reported.

Data availability

The data supporting this article have been included as part of the supplementary information (SI). Supplementary information is available. See DOI: **https://doi.org/10.1039/d5ta07333b**.

Acknowledgements

This research was funded by the Department of Energy's Office of Energy Efficiency and Renewable Energy (EERE) under the Building Energy Efficiency Frontiers in Innovation Technologies Program, Award Number DE-EE0009701. The authors also acknowledge support from the National Science Foundation

(CHE1429768) for the acquisition of the X-ray diffractometer. SEM-EDX analysis was conducted at the Mackay Microbeam Laboratory at UNR, with special thanks to Joel Desormeau for his assistance. We also acknowledge the Shared Instrument Laboratory in the Department of Chemistry at UNR.

References

1 U.S. Energy Information Administration, Monthly Energy Review, 2020, **https://www.eia.gov/totalenergy/data/monthly/archive/00352007.pdf**, accessed: January 2021.
2 E. Lee, M. Yazdanian and S. Selkowitz, *The Energy-Savings Potential of Electrochromic Windows in the UScommercial Buildings Sector*, Lawrence Berkeley National Laboratory (LBNL), Berkeley, CA (United States), 2004.
3 T. Cottineau, M. Toupin, T. Delahaye, T. Brousse and D. Bélanger, *Appl. Phys. A*, 2006, **82**, 599–606.
4 A. Malinauskas, J. Malinauskiene and A. Ramanavičius, *Nanotechnology*, 2005, **16**, R51.
5 S. Kanagaraj, A. Puthanveedu and Y. Choe, *Adv. Funct. Mater.*, 2020, **30**, 1907126.
6 L. Shao, X. Zhuo and J. Wang, *Adv. Mater.*, 2018, **30**, 1704338.
7 C. J. Barile, D. J. Slotcavage, J. Hou, M. T. Strand, T. S. Hernandez and M. D. McGehee, *Joule*, 2017, **1**, 133–145.
8 N. C. Bhoumik, S. M. Thompson and C. J. Barile, *Nano Energy*, 2024, **126**, 109710.
9 N. C. Bhoumik, D. C. Madu, C. W. Moon, L. S. Arvisu, M. D. McGehee and C. J. Barile, *Joule*, 2024, (8), 1.
10 N. C. Bhoumik, C. R. Potts, T. S. Hernandez and C. J. Barile, *Device*, 2024, **2**, 100412.
11 ASTM International, *ASTM E2141-21, Standard Test Method for Accelerated Aging of Electrochromic Devices in Sealed Insulating Glass Units*, West Conshohocken, PA, 2021.
12 N. Khanafi-Benghalem and K. Benghalem, *Opt. Laser Technol.*, 2011, **43**, 748–753.
13 T. A. Saleh, Interface Science and Technology, *Elsevier*, 2022, **34**, 233–263.
14 R. Solmaz and B. D. Karahan, *Int. J. Miner., Metall. Mater.*, 2020, **27**, 74–82.
15 S. Saravanan and K. Raghukandan, *Trans. Nonferrous Met. Soc. China*, 2022, **32**, 91–103.
16 J. Xiao, Q. Li, Y. Bi, M. Cai, B. Dunn, T. Glossmann, J. Liu, T. Osaka, R. Sugiura, B. Wu, J. Yang, J.-G. Zhang and M. S. Whittingham, *Nat. Energy*, 2020, **5**, 561–568.
17 J. Wang, Y. Lv, Y. Zhou, S. Jia, F. Zhu, O. G. Schmidt and G. Cai, *APL Energy*, 2024, **2**, 026104.
18 G. Rodríguez-Gattorno, P. Santiago-Jacinto, L. Rendon-Vázquez, J. Németh, I. Dékány and D. Díaz, *J. Phys. Chem. B*, 2003, **107**, 12597–12604.
19 Z. Qiu, Y. Nadamura and T. Ishiguro, *Thin Solid Films*, 2010, **518**, 5912–5915.
20 *CRC Handbook of Chemistry and Physics: A Ready-Reference Book of Chemical and Physical Data*, ed. W. M. Haynes, CRC Press, Boca Raton, FL, 97th edn, 2016.
21 R. M. Smith and A. E. Martell, *Critical Stability Constants: Second Supplement*, Springer, New York, 1989.
22 R. N. Goldberg, N. Kishore and R. M. Lennen, *J. Phys. Chem. Ref. Data*, 2002, **31**, 231–370.
23 M. A. Fernandez and R. H. de Rossi, *J. Org. Chem.*, 1999, **64**, 6000–6004.
24 T. D. N. Reddy and B. S. Mallik, *Comput. Theor. Chem.*, 2020, **1172**, 112663.
25 C. J. Moll, A. A. Korotkevich, J. Versluis and H. J. Bakker, *Phys. Chem. Chem. Phys.*, 2022, **24**, 10134–10139.
26 M. M. Voron, M. A. Fon Pruss and O. Y. Byba, *Cast. Processes*, 2021, **3**, 61–68.
27 L. Xin, G. Shao, F. Wang, P. Tsakiropoulos and T. Li, *Intermetallics*, 2003, **11**, 651–660.
28 S.-B. Wang, Q. Ran, R.-Q. Yao, H. Shi, Z. Wen, M. Zhao, X.-Y. Lang and Q. Jiang, *Nat. Commun.*, 2020, **11**, 1634.
29 Y. Zhao, S. Guo, M. Chen, B. Lu, X. Zhang, S. Liang and J. Zhou, *Nat. Commun.*, 2023, **14**, 7080.
30 M. Chen, Y. Gong, Y. Zhao, Y. Song, Y. Tang, Z. Zeng, S. Liang, P. Zhou, B. Lu and X. Zhang, *Natl. Sci. Rev.*, 2024, nwae205.
31 H. Tian, G. Feng, Q. Wang, Z. Li, W. Zhang, M. Lucero, Z. Feng, Z.-L. Wang, Y. Zhang, C. Zhen, M. Gu, X. Shan and Y. Yang, *Nat. Commun.*, 2022, **13**, 7448.
32 T. Wang, Q. Xi, K. Yao, Y. Liu, H. Fu, V. S. Kavarthapu, J. K. Lee, S. Tang, D. Fattakhova-Rohlfing and W. Ai, *Nano-Micro Lett.*, 2024, **16**, 112.
33 A. Brenner, *Electrodeposition of Alloys: Principles and Practice*, Elsevier, Amsterdam, 2013.
34 W. Kao-ian, M. T. Nguyen, T. Yonezawa, R. Pornprasertsuk, J. Qin, S. Siwamogsatham and S. Kheawhom, *Mater. Today Energy*, 2021, **21**, 100738.
35 D. C. Madu, S. M. Islam, H. Pan and C. J. Barile, *J. Mater. Chem. C*, 2021, **9**, 6297–6307.
36 A. J. Bard, L. R. Faulkner and H. S. White, *Electrochemical Methods: Fundamentals and Applications*, John Wiley & Sons, Hoboken, NJ, 3rd edn, 2022.
37 Y. Salhi, S. Cherrouf, M. Cherkaoui and K. Abdelouahdi, *Appl. Surf. Sci.*, 2016, **370**, 108–115.
38 D. Guan, J. Li, X. Gao and C. Yuan, *J. Alloys Compd.*, 2014, **617**, 464–471.
39 G.-W. Peng, X.-P. Gan, Z. Li and K.-C. Zhou, *Chin. Phys. B*, 2018, **27**, 086302.
40 H. W. King, *J. Mater. Sci.*, 1966, **1**, 79–90.
41 J. Malathi, M. Kumaravadivel, G. Brahmanandhan, M. Hema, R. Baskaran and S. Selvasekarapandian, *J. Non-Cryst. Solids*, 2010, **356**, 2277–2281.
42 Q. Zhang, Q. Li, D. Liu, X. Zhang and X. Lang, *J. Mol. Liq.*, 2018, **249**, 1097–1106.
43 M. T. Strand, T. S. Hernandez, M. G. Danner, A. L. Yeang, N. Jarvey, C. J. Barile and M. D. McGehee, *Nat. Energy*, 2021, **6**, 546–554.
44 M. J. Kalani, M. Salay Naderi and G. B. Gharehpetian, *Comput. Electr. Eng.*, 2019, **77**, 191–204.
45 M. T. Strand, C. J. Barile, T. S. Hernandez, T. E. Dayrit, L. Bertoluzzi, D. J. Slotcavage and M. D. McGehee, *ACS Energy Lett.*, 2018, **3**, 2823–2828.